Journal of Hydrology 617 (2023) 128898

Contents lists available at ScienceDirect

Journal of Hydrology

journal homepage: www.elsevier.com/locate/jhydrol

Research papers

Flow partitioning modelling using high-resolution electrical conductivity data during variable flow conditions in a tropical montane catchment

Patricio X. Lazo [a,*], Giovanny M. Mosquera [b], Irene Cárdenas [a], Catalina Segura [c], Patricio Crespo [a]

[a] Departamento de Recursos Hídricos y Ciencias Ambientales, Facultad de Ingeniería & Facultad de Ciencias Químicas, Universidad de Cuenca, Av. 12 de Abril, Cuenca, Ecuador
[b] Instituto Biósfera, Universidad San Francisco de Quito USFQ, Diego Robles y Vía Interoceánica, Quito, Ecuador
[c] Department of Forest Engineering, Resources, and Management, Oregon State University, Corvallis, OR, USA

ARTICLE INFO

This manuscript was handled by Marco Borga, Editor-in-Chief, with the assistance of Francesco Comiti, Associate Editor

Keywords:
Event and pre-event water
Hydrograph separation
Tracers
Rainfall-runoff events
Páramo

ABSTRACT

Tracer-aided hydrological models (TAHMs) are one of the most powerful tools to identify new (event) and old (pre-event) water fractions contributing to stormflow because they account both for streamflow and tracer mixing dynamics in model calibration. Nevertheless, their representativeness of hydrograph dynamics is often limited due to the unavailability of high-resolution conservative tracer data (e.g., water stable isotopes or chloride). Hence, there is a need to identify alternative tracers yielding similar flow partitioning results than "ideal" ones while requiring fewer financial resources for high-frequency monitoring (e.g., sub-hourly). Here, we compare flow partitioning results of a TAHM calibrated using high-frequency electrical conductivity (EC) and water stable isotope (^{18}O) data collected during 37 rainfall-runoff events monitored during variable hydrometeorological conditions in the Zhurucay Ecohydrological Observatory, a tropical alpine catchment located in southern Ecuador. When the model was calibrated using the sampling resolution of stables isotopes (6-hours to 1-hour), no statistically significant differences of pre-event water fractions (PEWFs) using both tracers for model calibration were found. PEWF differences between both tracers for 89% of the events were $< 20\%$ regardless of the events' antecedent moisture and rainfall conditions. Model transfer functions were also similar suggesting that catchment internal processes inferred using both tracers are comparable. Events presenting larger differences ($n = 4$; up to 27% PEWF difference) had no samples collected during peak flow. Calibration of the model using EC data collected at sub-hourly intervals (every 5-minutes) showed a significant increase in model performance as compared to the frequency of collection of isotopic data. Similarity in flow partitioning results can be attributed to a quasi-conservative nature of EC due to the presence of organic-rich riparian soils (peat-type) overlying compact bedrock across the catchment. Findings also highlight the importance of capturing rapidly occurring catchment mixing processes though high-temporal frequency monitoring of tracer data. Our study encourages the value of assessing the use of alternative tracers, such as EC, to identify fast occurring rainfall-runoff processes, while lowering the costs needed to implement and sustain tracer data collection for long time periods.

1. Introduction

Hydrological flow partitioning can be defined as the separation of precipitation into different water storage components and resulting fluxes in a catchment (Shope, 2016). Event hydrograph separation is one of the most common flow partitioning approaches. Such separations assume that stormflow can be divided in two (or more) flow components, event water—entering a hydrological system during a rainstorm event (precipitation) and pre-event water—stored in the system before the beginning of an event (soil or groundwater) (Buttle, 1994; Klaus and McDonnell, 2013; Pearce et al., 1986; Sklash and Farvolden, 1979). Determining these temporal flow components has proven useful across catchments to conceptualize rainfall-runoff processes (e.g., Goller et al., 2005; Hrachowitz et al., 2011; St Amour et al., 2005), identify surface and subsurface flow paths of water (e.g., Camacho Suarez et al., 2015; Laudon et al., 2004; Pearce et al., 1986), and determine runoff

* Corresponding author.
E-mail addresses: patricio.lazoj@ucuenca.edu.ec (P.X. Lazo), segurac@oregonstate.edu (C. Segura).

https://doi.org/10.1016/j.jhydrol.2022.128898
Received 31 March 2022; Received in revised form 18 November 2022; Accepted 27 November 2022
Available online 13 December 2022

generation thresholds (McGlynn and McDonnell, 2003; McGuire and McDonnell, 2010; Tweed et al., 2016).

Hydrograph separation approaches can be divided into three categories (Gonzales et al., 2009): i) empirical and numerical methods based on graphical analysis of hydrographs (e.g., Linsley et al., 1982) and low-pass numerical filtering (e.g., Chapman, 1999; Romanowicz, 2010; Su et al., 2016), ii) conceptual methods based on the idea that the catchment can be represented as conceptual reservoirs interconnected (e.g., Michel et al., 2003; Wittenberg, 1999; Wittenberg and Sivapalan, 1999), and iii) tracer-based methods which are a combination of the conceptual methods where the calibration of the model depends on streamflow and tracer concentration (e.g., Christophersen and Hooper, 1992; Laudon and Slaymaker, 1997; Muñoz-Villers and McDonnell, 2012). The latter one, based on physical principles (i.e., mass balance) (Mei and Anagnostou, 2015; Miller et al., 2014; Zhang et al., 2017) and isotopic or geochemical (tracer) signals measured directly on water fluxes and/or storages (Klaus and McDonnell, 2013) is one of the most robust methodologies. However, mass balance mixing models have limited potential to integrate runoff and tracer response to precipitation inputs (Birkel et al., 2014) because they do not provide a representation of internal processes or flowpaths. In response to this limitation, approaches integrating tracer information for the calibration of numerical flow models have been developed (Benettin et al., 2015, 2013; Birkel et al., 2011; McGuire et al., 2007). Simultaneous calibration of flow transport and tracer mixing not only improves the realism of models compared to calibration with streamflow alone (Soulsby et al., 2015; Stadnyk et al., 2013; Vaché and McDonnell, 2006), but also results in more constrained parameter values (Wang et al., 2018, Wang et al., 2017). Tracer-aided modelling has allowed refined understanding of catchment hydrological functioning by simultaneously accounting for streamflow and tracer mixing dynamics into model calibration (e.g., Mosquera et al., 2018; Segura et al., 2012; Weiler et al., 2003).

Several tracers have been used for event hydrograph separation but despite their limitations (Buttle, 1994; (Klaus and McDonnell, 2013)), water stable isotope ratios of oxygen and hydrogen ($\delta^{18}O$ and $\delta^{2}H$) are considered to be ideal tracers because of their conservative nature when not influenced by evaporative processes (Klaus and McDonnell, 2013). However high resolution isotopic data remains challenging to obtain and records are limited in most cases to a few months (Wang et al., 2019). Hence, there is a need to identify alternative tracers. Electrical conductivity (EC)—defined as a measure of the ability of water to transfer an electrical current—has been alternatively used in flow partitioning studies (e.g., Lott and Stewart, 2016; Munyaneza et al., 2012; Stewart et al., 2007) due to its low monitoring and maintenance cost. It can easily be collected at sub-hourly temporal frequency (e.g., Mosquera et al., 2018). Although EC is considered as a non-conservative tracer because of its dependence on catchment geochemical processes which limit its use in hydrograph separation studies (e.g., Blume et al., 2008; Hayashi et al., 2012; Pearce et al., 1986), it has also been reported to provide similar flow partitioning results compared with stable isotopes in different environments worldwide (e.g., Camacho Suarez et al., 2015; Cano-Paoli et al., 2019; Meriano et al., 2011; Vidon and Cuadra, 2010). A recent study revealed a high level of agreement between flow partitioning results using a tracer-aided hydrological model calibrated for stable isotopes and EC for a rainfall event in a catchment with Mediterranean climate in Oregon, USA (Mosquera et al., 2018). These findings encourage the use of tracer-aided hydrological modelling to assess whether EC recorded at high temporal frequency can be used as a surrogate for conservative tracers in hydrograph separation studies (Cano-Paoli et al., 2019; Saraiva Okello et al., 2018). In this paper we used water stable isotope ratios and EC data monitored at high-temporal frequency (sub-daily to sub-hourly) during 37 rainfall-runoff events at the Zhurucay Ecohydrological Observatory, a tropical mountain catchment located in southern Ecuador to:

i) assess whether the calibration of a tracer-aided hydrological model using EC and stable isotopes for events monitored under variable hydrometeorological conditions yield similar hydrograph separation results, and,
ii) evaluate how model calibration using EC data collected at sub-hourly intervals (every 5-minutes) influences model performance.

2. Materials and methods

2.1. Study site

The study site is a tropical alpine (páramo) catchment located within the Zhurucay Ecohydrological Observatory (ZEO) on the west slope of the Atlantic-Pacific continental divide in the Andes of southern Ecuador (3°04′ S, 79°14′ W) (Fig. 1). The catchment is 3.28 km^2 and varies in elevation between 3,676 and 3,900 m.a.s.l. Climate is influenced by air masses stemming from the Amazon rainforest (Esquivel-Hernández et al., 2019), presenting a mean annual precipitation of 1,345 mm at 3,780 m.a.s.l. Rainfall occurs almost daily as drizzle with rain intensities rarely exceeding 5 mm/h (Padrón et al., 2015). Despite the high-elevation of the study site, its geographical location at a tropical latitude near the equator precludes the occurrence of snow. The catchment presents flashy discharge response to precipitation (Mosquera et al., 2016a, Mosquera et al., 2015), which has been linked to frequent water occurrence of saturated conditions at the thin soils (usually < 1 m depth) as a result of their high water retention capacity and the constant input of low intensity precipitation (Lazo et al., 2019). Hydrology in the system is dominated by shallow subsurface flow (Mosquera et al., 2016b). Monitoring at 3,780 m.a.s.l indicate mean annual temperature of 6 °C, 90% relative humidity, and reference evapotranspiration of 2 mm/day (Córdova et al., 2015).

Two geological formations dominate the study site, the Quimsacocha and Turi formations. The Quimsacocha presents basaltic flows with plagioclases, feldspars, and andesitic pyroclastics. The Turi is composed of tuffaceos andesitic breccias, conglomerates, and horizontal stratified sands. Soils in the ZEO are rich in organic matter, black, humic, and acid, with high water storage capacity (Quichimbo et al., 2012). They formed from the accumulation of volcanic ash over low gradient slopes and valley bottoms. They are identified as Andosols and Histosols (IUSS Working Group WRB, 2015), covering 74% and 26% of the study area, respectively (Mosquera et al., 2015). The depth of the soil ranges between 0.9 m and 2.0 m for the Histosols, and between 0.2 m and 0.7 m for the Andosols, with a slightly weathered underlying shallow bedrock above compact bedrock. The ZEO is mainly composed of two types of vegetation: 1) tussock grasses (*Calamagrostis* sp.) covering the Andosols and 2) cushion plants (*Plantago rigida, Xenophyllum humile, Azorella* spp.) overlying the Histosols. The latter vegetation-soil combination was defined as "Andean Wetlands" by Mosquera et al. (2016a). The study area is mostly undisturbed with light grazing mainly in the lower part of the catchment (Mosquera et al., 2015).

2.2. Hydrometric data collection

Water level and precipitation data were collected during the period October-2017 to June-2019. Water level data at the catchment outlet (Fig. 1) were recorded using a V-notch weir equipped with an INW (AquiStar CT2X, Kirkland, WA, USA) pressure transducer (accuracy of +/- 1.75 mm). The constant rate salt dilution method (Moore, 2004) was used to calibrate the Kindsvater-Shen equations (U.S. Bureau of Reclamation, 2001) to convert water level data into discharge (Guallpa et al., 2022). Precipitation was measured using 4 HOBO (RG3-M, Onset Computer Corporation, Bourne, MA, USA) rain gauge tipping buckets (0.2 mm resolution) distributed across the catchment (Fig. 1).

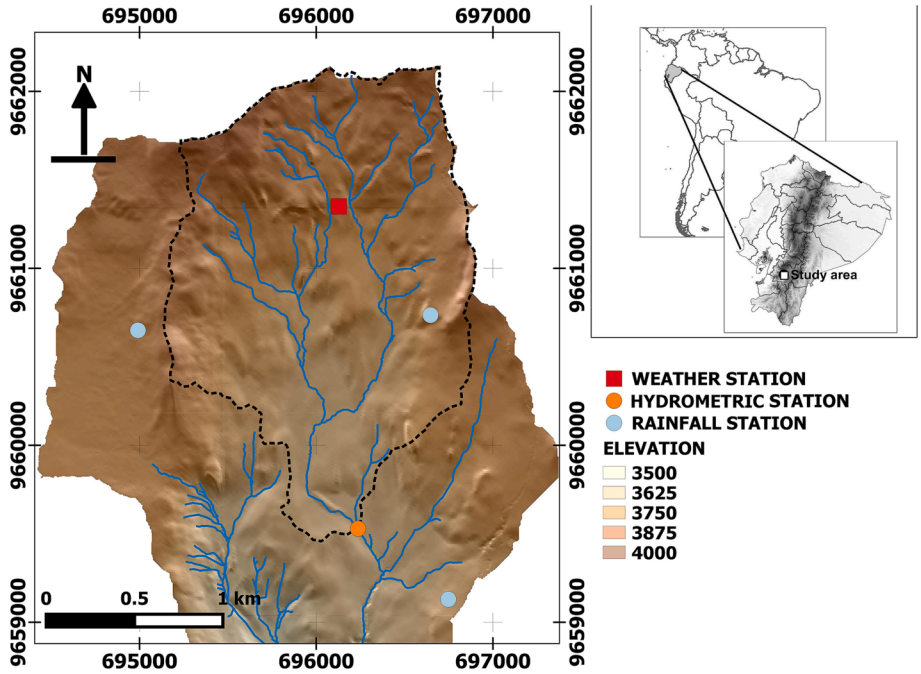

Fig. 1. Map of the study site located at the Zhurucay Ecohydrological Observatory (ZEO) in south Ecuador showing the hydrometeorological monitoring setup.

2.3. Tracer data collection

Water samples for Oxygen-18 analysis were collected during the same period as hydrometric data (i.e., October-2017 to June-2019). Discharge samples were collected at the catchment outlet (Fig. 1) using a PVS4120D autosampler (Campbell Scientific, Logan, UT, USA). Sampling interval varied depending on available logistical resources. Three sampling intervals were applied as follows: from October-2017 to January-2018 sampling interval was every 6 h, from January-2018 to March-2019 samples were collected every 4 h, and from March-2019 to June-2019 the sampling interval was hourly.

Precipitation samples were collected using a volumetric sequential rainfall sampler (Fig S1) located near the meteorological station in the upper part of the catchment (Fig. 1). The collector was free from evaporative fractionation as indicated by the oxygen-18 and deuterium relation (Fig. S2). Both discharge and precipitation water samples were collected and stored in 2 ml amber glass bottles. Discharge water samples were filtered in situ using 0.45 μm polypropylene single-use syringe membrane filters (Puradisc 25 PP Whatman Inc., Clifton, NJ, USA). The bottles were sealed with parafilm and stored away from sunlight to avoid evaporative fractionation effects.

Oxygen-18 isotopic composition was measured using a cavity ring-down spectrometer (Picarro 2130-i). Precipitation and discharge samples were analyzed in separate runs in order to diminish memory effect in the analysis (Penna et al., 2012). Six sample injections were applied and the first three were discarded to further reduce memory effects. In order to control the quality of the analysis, a set of three isotopic standards were analyzed every 12 samples, obtaining strong linear correlations ($r^2 > 0.99$). In addition, the standards' error (0.1 ‰) and the error of the analysis (0.1 ‰), both reported by the manufacturer, were added (0.2 ‰), and if the average error of the three measurements resulting from the standards' injections was larger than such value, the samples were reanalyzed. This procedure was undertaken for each set of standards analyzed. The samples were checked for organic contamination using ChemCorrect™ (Picarro Inc., Santa Clara, CA, USA). We used the δ notation for reporting the isotopic composition in per mill (‰) using the Vienna Standard Mean Ocean Water (V-SMOW; Craig, 1961) as reference.

Electrical Conductivity (EC) was measured in precipitation and stream water. Discharge EC values were recorded at the catchment outlet through the same probe used for water level monitoring (i.e., INW CT2X, accuracy of ± 0.5% of the measured EC value). EC data were recorded at the same sampling resolution as water level data (i.e., every 5 min) and are expressed in μS/cm. The probe was calibrated prior to installation and every 6 months afterwards to secure high quality of the data. Water samples to determine precipitation EC were collected using the aforementioned volumetric sequential rainfall sampler. EC water samples were collected at the same time water samples for isotope analysis were taken but stored in 50 ml plastic bottles. Subsequently, EC was measured in each water sample using a WTW Universal Multi-Parameter (Handheld ProfiLine Multi 3320, Xylem Analytics Germany GmbH, Weilheim, Germany) equipped with a conductivity measuring cell (TetraCon 325, Xylem Analytics Germany GmbH, Weilheim, Germany) with an accuracy of ± 0.5% of the measured value. The calibration of the equipment was performed before every sampling campaign.

2.4. Rainfall-runoff events selection and characterization

Rainfall-runoff events were selected using hydrometric data to analyze event and pre-event flow partitioning under variable flow conditions. Events were defined using the Peak Over Threshold (POT) method in which the sample is all peak values above a baseline discharge threshold (Lang et al., 1999). The threshold selected was the ZEO low flow value corresponding to the Q35 non-exceedance flow rate (Mosquera et al., 2015). Thus, runoff response to rainfall starting below Q35 with peak values over this threshold were considered as rainfall-runoff events. Additionally, a minimum inter-event criteria (Dunkerley, 2008) was also used to select events accounting for precipitation dynamic. The minimum inter-event time to define independent events was 6 h due to the frequent occurrence of rainfall at the ZEO (Padrón et al., 2015). Analyses were conducted using R version 3.5.1 with the POT package (Ribatet and Dutang, 2004).

The following variables were estimated to characterize the selected rainfall-runoff events: peak flow, cumulative discharge, cumulative precipitation, and runoff coefficient. These variables allowed evaluation of the flow conditions under which flow partitioning was carried out at the ZEO. Additionally, we assessed the streamflow sampling resolution

as the ratio of the number of samples collected during each of the events to the event duration in hours. This allowed us to evaluate the influence of sampling resolution on flow partitioning results.

2.5. Tracer-aided flow partitioning modelling

We used the Tracer-based Streamflow Partitioning Analysis model (TraSPAN; Mosquera et al., 2018) to estimate event and pre-event water fractions for each rainfall-runoff event. TraSPAN is an event-based model that uses a combination of the unit hydrograph approach to simulate discharge response to rainfall events and flow response transit time distributions (TTDs) to account for internal catchment mixing processes through tracer mass balance.

In the following, we describe the main features of TraSPAN, and the reader is referred to Mosquera et al. (2018) for a detailed description of the modelling framework. TraSPAN is composed of three modules (Table S1 and Fig S3). The first module computes effective rainfall (P_{eff}) as the product of antecedent rainfall index (s) (Jakeman and Hornberger, 1993) and precipitation (P) (Equations 1 and 2 in Table S1). The second module calculates the fraction of P_{eff} routed as event or pre-event water. Module 3 estimates the event (Q_e) and pre-event (Q_p) water fractions through convolution of the TTDs. Convolution results are used in combination with a mass balance approach to estimate the tracer concentration (Equation 8 in Table S1). The sum of Q_e and Q_p represents total discharge (Q).

Modules 2 and 3 allow for the configuration of different structures representing different catchment hydrological behavior. Module 2 permits setting up the fraction (f) of P_{eff} that is routed as event water to be constant or time-variant (Equation 3 in Table S1). Module 3 gives the possibility to select between two TTDs commonly used to assess the representation of tracer mixing in hydrological models: the Exponential Model (EM; Maloszewski and Zuber, 1996) which represents a single linear reservoir (Equations 6 and 7 in Table S1) and the Two Parallel Linear Reservoir model (TPLR; Weiler et al., 2003) which consists of two connected linear reservoirs (Equations 9 and 10 in Table S1). The combination of the different options of modules 2 and 3 results in four possible model structures. Structure 1 uses f as constant and the EM TTD to estimate event and pre-event fractions (7 calibration parameters). Structure 2 also considers f as constant but uses the TPLR TTD for flow partitioning (11 calibration parameters). Structure 3 assumes f as a time-variant function with the EM TTD for event and pre-event water estimation (8 calibration parameters). Structure 4 assumes f as a time-variant function in combination with the TPLR model (12 calibration parameters). The equations and calibration parameters for each model structure are presented in Table S1 and Fig. S3 as they are described in detail in Mosquera et al. (2018).

The pre-event end-member concentration was estimated as the average of the three streamflow samples collected prior to the beginning of the events (Bonell et al., 1990). The event end-member concentration was assumed equal to the incremental weighted mean of precipitation samples collected during the events (McDonnell et al., 1990).

2.6. Model evaluation and selection of best model structure

We ran the four model structures for each rainfall-runoff event using either $\delta^{18}O$ and EC for calibration. Each model structure was run a million times. A Monte-Carlo sampling approach was used to produce a set of randomly generated parameter values for each model run (Beven and Freer, 2001). The range of values from which the parameter sets were defined was selected according to values commonly found in the published literature (e.g., Mosquera et al., 2018; Segura et al., 2012; Weiler et al., 2003). The same time steps for hydrometric and tracer data were used to allow for a direct comparison of the model calibration results using $\delta^{18}O$ and EC. Hydrometric data (precipitation and discharge) at 5 min intervals were used. Considering the different sampling resolution of isotopic (6 h, 4 h, and hourly; Section 2.3), and EC (every 5 min) data, only EC data collected at the same time than $\delta^{18}O$ data were used for comparing flow partitioning results. EC and $\delta^{18}O$ data in precipitation were volume weighted to aggregate them to the same frequency tracer data in streamflow where available.

The Kling-Gupta Efficiency (KGE; Gupta et al., 2009) metric was used to evaluate the goodness of fit of the model simulations to the hydrometric and tracer observations. For comparison among the four model structures, we used the average of the discharge and tracer KGE values (Mosquera et al., 2018). The Akaike Information Criteria (AIC; Akaike, 1974) metric was calculated to evaluate the parsimoniousness of each of the model structures to account for their different number of calibration parameters. The discharge and tracer AIC values were added into a single one to compare the different model structures (Mosquera et al., 2018). The model structure presenting the highest KGE and lowest AIC values was considered as the best representation ("best model structure") of the hydrological behavior of the catchment for each rainfall-runoff event. Uncertainty of the results was obtained using a threshold of behavioral solutions. This threshold included sets of parameters yielding KGEs above 0.5, except when the best KGE for the event was $<$ 0.5 for which the threshold was set in KGEs above 0.3. We obtained$>$5000 behavioral sets for all analyzed events.

The KGE and AIC metrics were used to compare whether the best model structures calibrated using $\delta^{18}O$ and EC yielded similar flow partitioning results. To this end, we assessed the difference between the pre-event water fractions estimated for the best model structure using $\delta^{18}O$ and EC separately for calibration. If such difference was lower than 20%, the results were considered as similar (Laudon and Slaymaker, 1997). Uncertainty in the modelling results was considered in the comparison by calculating the difference of pre-event water fractions of the 5 and 95% confidence limits from the parameter sets within the range of behavioral solutions. Furthermore, statistical significance of the differences between the pre-event water fractions estimated using $\delta^{18}O$ and EC was evaluated using the Sign (Sprent, 2011) and Wilcoxon signed-rank test (Wilcoxon, 1945) to a significance level of 0.05 (α = 0.05), and the statistical power of these tests, representing the probability that they correctly rejected the null hypothesis, was also assessed. The effect size for the statistical power analysis was obtained using the formula $r = Z/\sqrt{N}$ following the guidelines proposed by Tomczak and Tomczak (2014), where Z equals the z-value, N is the number of paired samples, and r refers to the effect size. We visually inspected the TTDs produced by the best model structure calibrated for each tracer during each rainfall-runoff event to evaluate if the modelling results yielded a similar representation of the catchments' transport and mixing processes for different flow conditions.

2.7. Influence of temporal data collection frequency on flow partitioning

Taking advantage of the high temporal frequency at which EC data were collected, we tested the influence of sampling frequency on flow partitioning results. To this end, the simulations were carried out using the original temporal resolution at which EC and discharge data were collected during each rainfall-runoff event, i.e., every 5 min. Precipitation data were also aggregated to the same time frequency. We compared the results obtained with high frequency data (5 min) against those resulting when the model was run using EC data at the same frequency $\delta^{18}O$ data were available (6 h to hourly). The KGE metric was used to evaluate whether the use of high-frequency data influences the goodness of fit of the model results.

3. Results

3.1. Rainstorm events characterization

Thirty-seven rainfall-runoff events were monitored during the study period over a wide range of hydrometeorological conditions. Peak flow

varied from 0.02 to 2.1 mm/h (Table 1, Fig. 2). Events were ordered and labeled in ascending order according to their position over this curve. Events lasted between 10 and 104 h (Table 1). Events lasting > 70 h mainly produced low peak flows (events 1–4), except for event 21 (70 h) that yielded a moderate peak flow (0.3 mm/h). The duration of the rest of the events was<52 h (2.17 days). Cumulative precipitation during the events ranged between 2.9 and 26.2 mm with cumulative discharge values varying between 0.6 and 22.7 mm (Table 1). The variation of the runoff coefficient of the events was large and ranged between 0.05 (event 1) and 0.92 (event 20) most likely as a result of the varying rainfall-runoff response and antecedent moisture conditions in the catchment.

3.2. Selection of best model structure

The four evaluated model structures for all events calibrated using $\delta^{18}O$ yielded KGE values varying between 0.23 and 0.94 (structure 1), 0.07 and 0.86 (structure 2), 0.20 and 0.89 (structure 3), and 0.28 and 0.90 (structure 4) (Fig. 3a). This, except for event 18 using model structure 3 for which no set of parameters produced KGE values > 0, although we found no specific event features (e.g., peak flow, cumulative discharge and rainfall, antecedent precipitation) explaining this observation. Event 23 presented the highest KGE for all model structures, whereas event 5 had the lowest KGE for structures 1, 3, and 4 and event 33 produced the lowest KGE for structure 2. About 80% of the events (n = 29) had KGEs > 0.5, and model structures 1 and 4 had the largest number of events with KGE > 0.5 (Fig. 3a). Most KGE differences between model structures 1 and 4 were smaller than 0.06. The lowest AIC values corresponded to structures 2 and 4 (Fig. 3b). Overall, the combined evaluation of the KGE and AIC metrics showed that model structure 4 consistently yielded the highest KGE values (i.e., >0.6) and lowest AIC values for most events.

We also obtained good results (i.e., KGE > 0.5 for most events) when using EC for calibration. Similar to $\delta^{18}O$ calibration, only event 18 could not be calibrated using model structure 3 (KGE < 0). KGE values varied between 0.19 and 0.82 (structure 1), 0.3 and 0.81 (structure 2), 0.36 and 0.81 (structure 3), and 0.45 and 0.85 (structure 4) (Fig. 3c). All structures presented KGE values higher than 0.5, except for events 6 (0.47), 12 (0.42), and 16 (0.19) with structure 1, events 3, 5, 6, 12, 14, 15, and 16 for structure 2 with KGE 0.16–0.48, events 12 (0.36) and 16 (0.42) with structure 3, and event 6 (0.45), 12 (0.45), and 16 (0.46) for structure 4. Model structure 4 had the highest KGE values for 22 of the 37 events and was very close to the highest KGE values for the rest of the events with differences usually smaller than 0.05 compared with the structures producing the highest KGEs (Fig. 3c). As with $\delta^{18}O$, AIC values indicated that structures 2 and 4 presented the lowest AIC values (Fig. 3d). These results indicate that model structure 4 is the one that best represents the rainfall-runoff dynamics of the catchment using EC for model calibration.

3.3. Flow partitioning modelling results

Pre-event water fractions (PEWFs) estimated using the model structure best representing the hydrological system with each tracers ($\delta^{18}O$ or EC) for model calibration (i.e., model structure 4) are presented in Fig. 4. The figure shows the PEWFs that yielded the highest KGE values and their associated uncertainties. In general, a dominance of PEWF (>50% of total stormflow) was observed for the simulations producing the highest KGEs regardless of the tracer used for model calibration. For $\delta^{18}O$ calibration, PEWFs ranged from 40.9% to 98.8% and only two events presented PEWFs < 50% (events 2 and 34). When the model was calibrated using EC, PEWFs varied between 22.4% and 96.7%, and only one event had a PEWF lower than 50% (event 2).

The median of the simulation uncertainties (i.e., 5–95 confidence intervals) obtained using $\delta^{18}O$ for calibration of structure 4 was 18.5% and ranged from 6.2% to 31.5%. The median of the uncertainties for the same model structure calibrated using EC was 23.2% and varied between 9.2% and 45.2%. It is worth highlighting that model structure 4 yielded the lowest PEWF uncertainties for all events using $\delta^{18}O$ and EC (Fig. S4). These results further support the selection of structure 4 as the one best representing the studied hydrological system. A dominance of PEWF in>70% of the event hydrographs was observed (Fig. 4).

3.4. Comparison of flow partitioning modelling using $\delta^{18}O$ and EC

Differences in PEWFs estimated using $\delta^{18}O$ and EC (i.e., $\delta^{18}O$ PEWF – EC PEWF) ranged from −17.45% to 27.26% for model structure 4 (Fig. 5). Thirty-three out of the 37 monitored events presented differences smaller than 20%, and 18 had differences lower than 10%. All events producing low peak flows yielded similar PEWF estimates regardless of the number of samples available during peak flow production (i.e., above 85% of the events' peak flow value) and their sampling resolution value (Fig. 5). The events showing differences > 20% had the commonality that no samples were collected during peak flow production and they had sampling resolution values lower than 0.25.

PEWFs calculated using $\delta^{18}O$ and EC were similar as depicted by the overlap of their associated uncertainties for most of the events, except for events 22 and 36. The Sign and Wilcoxon statistical tests showed no significant differences between the results obtained using $\delta^{18}O$ and EC for structure 4 (p-value > 0.05; 0.19 for Sign and 0.07 for the Wilcoxon; Table 2), with a 96% probability that the test correctly rejects the null hypothesis represented by the statistical power (Table 2). Although differences between PEWF estimations using structure 4 were the smallest among all evaluated models (Fig. S5), results showed that EC gave similar PEWF estimations than $\delta^{18}O$ regardless of the evaluated model structure. A remarkable similarity between the TTDs of event and pre-event water fractions using $\delta^{18}O$ and EC for model calibration was also observed (Fig. 6).

3.5. Effect of high frequency data in flow partitioning modelling

In order to assess how increasing the tracer temporal sampling resolution influences the goodness of fit of the model simulation results, we used the original EC sampling resolution (i.e., every 5-minutes) to estimate PEWFs for the 37 rainfall-runoff events using the best model structure of the system (i.e., structure 4). All of the events presented a considerable increase in their KGE values which varied between 0.54 (event 9) and 0.92 (event 16; Fig. 7). This represented an average KGE increase of 14% among all events in relation to the KGEs yielded when the simulations were carried out using the original $\delta^{18}O$ sampling resolution used to compare the PEWFs estimated using $\delta^{18}O$ and EC (i.e., 1 to 6 h). Uncertainty in the results showed an average decrease of 5% for all the events, with event 33 having the highest decrease (8%) and event 16 presenting the lowest reduction (2%).

4. Discussion

4.1. Selection of the best model structure and process-based conceptualization

Using two tracers for model calibration ($\delta^{18}O$ and EC), TraSPAN allowed evaluation of four model structures representing different catchment hydrological behavior (competing hypothesis; Pfister and Kirchner, 2017) for 37 rainfall-runoff events monitored for a wide range of climatological and flow conditions to obtain the best representation of the investigated hydrological system. Goodness of fit (KGE) analysis indicated that model structure 4 provided the best representation of the studied páramo catchment for 64% of all events regardless of the tracer used for model calibration (Fig. 3). These results were confirmed by the parsimony analysis which showed that model structure 4 presented the lowest AIC values despite it had the largest number of calibration

Table 1
Main hydrometeorological characteristics of the 37 monitored rainfall-runoff events. Events are ordered according to their peak flow value from minimum (Event 1) to maximum (Event 37).

Event code	Start date	End date	Duration (hour)	Peak flow (mm/h)	Cumulative rainfall (mm)	Cumulative discharge (mm)	Average rainfall intensity (mm/h)	Runoff coefficient	Number of discharge samples collected
1	04–01-2018 18:00	08–01-2018 18:00	96	0.02	10.3	0.6	0.1	0.05	17
2	29–12-2017 15:00	02–01-2018 23:00	104	0.03	13.9	1.0	0.1	0.07	15
3	05–10-2018 22:00	10–10-2018 5:00	103	0.03	12.8	1.3	0.1	0.10	26
4	19–03-2018 2:00	22–03-2018 19:00	89	0.04	15.3	1.6	0.2	0.10	15
5	01–06-2019 10:20	02–06-2019 15:30	29.17	0.16	6.0	2.7	0.2	0.46	25
6	04–06-2019 17:30	05–06-2019 10:10	16.67	0.16	6.7	2.1	0.4	0.31	15
7	07–05-2019 18:40	09–05-2019 4:00	33.33	0.16	6.9	3.5	0.2	0.50	17
8	02–03-2019 11:00	03–03-2019 12:00	25	0.17	5.2	2.4	0.2	0.46	3
9	24–03-2018 14:00	25–03-2018 18:00	28	0.18	6.0	2.1	0.2	0.35	5
10	29–03-2019 11:20	30–03-2019 5:40	18.33	0.19	9.2	1.9	0.5	0.21	5
11	21–04-2019 14:20	22–04-2019 12:00	21.67	0.21	8.8	2.4	0.4	0.27	16
12	12–02-2019 9:40	13–02-2019 7:20	21.67	0.22	6.1	3.2	0.3	0.53	5
13	01–02-2019 7:00	02–02-2019 16:20	33.33	0.22	11.0	3.5	0.3	0.32	7
14	28–04-2018 4:00	29–04-2018 10:00	30	0.22	8.9	4.4	0.3	0.49	6
15	01–05-2018 16:00	02–05-2018 23:00	31	0.22	10.5	4.2	0.3	0.4	6
16	20–11-2018 13:10	21–11-2018 14:10	25	0.24	8.6	2.0	0.4	0.23	7
17	04–04-2019 14:50	05–04-2019 7:30	16.67	0.25	2.9	2.6	0.2	0.88	5
18	22–10-2017 9:00	23–10-2017 9:00	24	0.25	8.1	2.8	0.3	0.35	6
19	07–04-2019 9:30	08–04-2019 14:40	29.17	0.27	8.4	3.3	0.3	0.39	9
20	23–04-2019 13:50	24–04-2019 9:50	20	0.30	3.5	3.2	0.2	0.92	20
21	29–07-2018 6:00	01–08-2018 4:00	70	0.33	16.7	8.0	0.2	0.48	18
22	21–03-2019 13:20	22–03-2019 10:10	20.83	0.34	10.2	3.3	0.5	0.33	6
23	01–08-2018 6:00	03–08-2018 10:00	52	0.40	8.9	6.4	0.2	0.72	12
24	09–02-2019 13:20	10–02-2019 7:40	18.33	0.49	9.	4.4	0.5	0.47	6
25	24–03-2019 12:10	25–03-2019 17:20	29.17	0.55	12.1	5.9	0.4	0.48	8
26	14–01-2018 8:00	15–01-2018 8:00	24	0.57	21.5	3.7	0.9	0.17	4
27	30–03-2018 19:00	31–03-2018 18:00	23	0.57	13.7	3.8	0.6	0.27	5
28	22–03-2019 11:00	23–03-2019 15:20	28.33	0.60	9.0	6.9	0.3	0.77	7
29	14–05-2019 17:20	15–05-2019 3:20	10	0.60	7.3	3.8	0.7	0.52	7
30	05–06-2019 10:10	06–06-2019 7:00	20.83	0.63	8.4	5.4	0.4	0.65	18
31	13–02-2019 10:40	14–02-2019 11:40	25	0.73	12.5	7.1	0.5	0.57	7
32	15–05-2019 5:50	15–05-2019 20:00	14.17	0.80	11.4	6.8	0.8	0.59	9
33	16–01-2018 14:00	18–01-2018 9:00	43	1.03	21.5	11.1	0.5	0.51	4
34	26–05-2018 10:00	27–05-2018 11:00	25	1.38	16.1	14.1	0.6	0.88	7
35	07–05-2018 9:00	08–05-2018 9:00	24	1.46	12.3	9.5	0.5	0.77	5
36	18–01-2018 11:00	19–01-2018 12:00	25	1.59	15.8	8.5	0.6	0.54	5
37	24–05-2018 11:00	25–05-2018 17:00	30	2.14	26.2	22.7	0.9	0.86	8

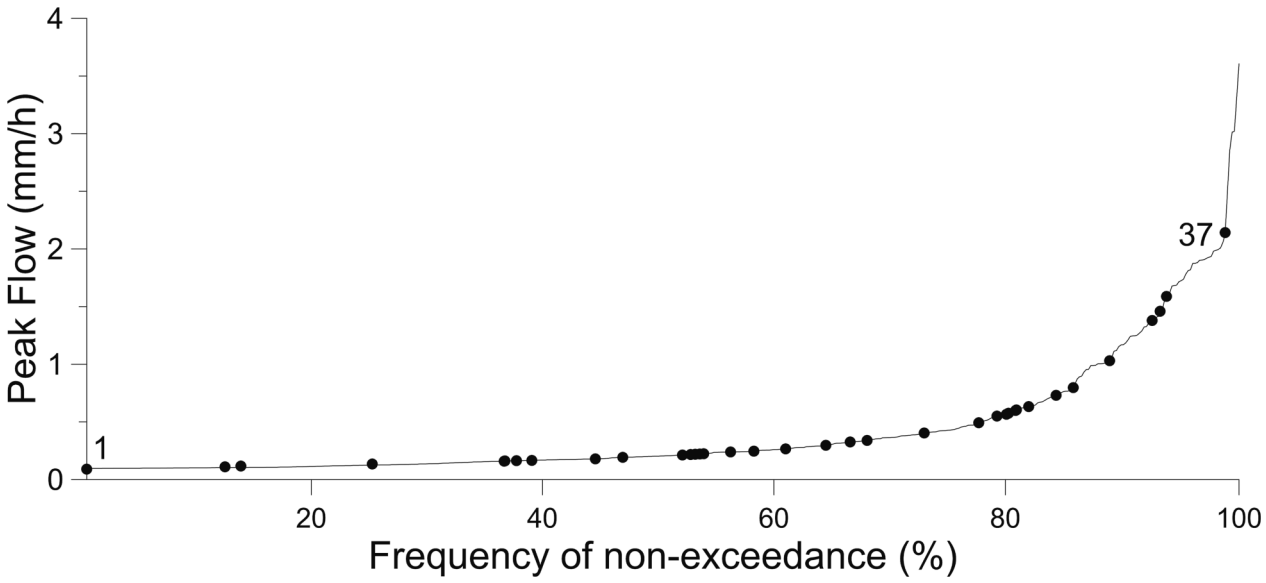

Fig. 2. Peak flow of the 37 monitored events along the peak flow non-exceedance curve constructed using 10-years of discharge data (2010–2020) at the study catchment. Black dots represent the peak flow value for each of the monitored rainfall-runoff events. Events were ordered according to their peak flow from minimum to maximum. That is, event 1 has the lowest peak flow, whereas event 37 has the highest one.

parameters of all the evaluated structures. This finding reassures that the selection of this model structure was not affected by over-parameterization issues (Forster, 2000).

The selection of this model structure is supported by the conceptualization of rainfall-runoff processes at the study catchment. Model structure 4 involves a variable fraction of effective precipitation routed as event water and 2 reservoirs with different travel times (fast and slow), where water mixes and is further released as streamflow. The time variable fraction of event water likely accounts for two processes. First, interception losses from tussock grasses covering 74% of the catchment (tussock grass water storage capacity = 2 mm) (Ochoa-Sánchez et al., 2018) as precipitation intensity during the monitored events rarely exceeded 0.5 mm/hr (Table 1). Second, the recharge of the available water storage in the riparian wetlands (Histosol soils) at the beginning of the events (Lazo et al., 2019).

The water reservoir with fast transfer time reflects a combination of direct channel precipitation (e.g., Penna et al., 2015) and water that flows in the first few centimeters of the paramo soils in the riparian wetlands which remain near saturation conditions year-round (Mosquera et al., 2015). That is, with little to no contact time with the subsurface (Delsman et al., 2013). These water flow paths on average account for 15% (using $\delta^{18}O$) and 22% (using EC) of storm runoff according to our tracer-based hydrograph separation estimations. They constitute the "new water" end-member of the system during stormflow generation (Correa et al., 2019). The reservoir with slow travel time represents the mobilization of water from deeper horizons of hillslope and wetland soils and small contribution from shallow groundwater in the rather compact bedrock (Correa et al., 2017; Crespo et al., 2011; Lazo et al., 2019). It represents the "old water" end-member dominating the stormflow hydrograph (on average 85% with $\delta^{18}O$ and 78% with EC).

The dominance of the PEWFs during rainfall events (Fig. 4) is in line with that reported based on weekly to biweekly data collected in the period 2011–2014 in the study area (PEWFs > 75%) (Correa et al., 2017; Mosquera et al., 2016a). The prevalence of pre-event water is also in agreement with the concept that runoff generation is mainly controlled by water stored in catchments prior to rainfall events (Klaus and McDonnell, 2013; McGuire and McDonnell, 2010; Muñoz-Villers and McDonnell, 2012). Overall, the selection of model structure 4 as the best representation of the catchment's hydrological behavior during rainfall-runoff events is supported by the statistical analysis and the mechanistic understanding of runoff generation at the study site.

4.2. Comparison of flow partitioning modelling using stable isotopic and EC data under variable flow conditions

The comparison of PEWFs estimated using model structure 4 showed that $\delta^{18}O$ and EC yielded similar flow partitioning results for most of the events (Fig. 5). Such similarity of flow partitioning results between both tracers has also been reported in a variety of catchments worldwide. Vidon and Cuadra (2010) found differences between 5% and 15% at a tile-drained field site in the USA. Laudon and Slaymaker (1997) obtained differences of about 20% in alpine catchments in British Columbia. Cano-Paoli et al. (2019) analyzed hydrograph separation at a headwater alpine catchment in Italy, where the differences between estimations yielded by the two tracers were about 10%. Camacho Suarez et al., (2015) reported no major differences (<9%) in a sub-tropical semi-arid environment. Meriano et al. (2011) also found small differences (8%) at an urban glaciated catchment in Canada. It is worth noting that the aforementioned investigations were conducted using a rather limited number of monitored events, normally<10. This limitation reduced the capacity to statistically evaluate the significance of the reported similarities, as well as potential differences in results over a wide range of climatological and flow conditions. The unique dataset presented in this study permitted to statistically support our findings (Table 2), which in general did not depend on such hydroclimatological variability.

It is well known that EC can behave as a non-conservative tracer under certain conditions (Hayashi et al., 2012; Laudon and Slaymaker, 1997; Pellerin et al., 2008). In other tropical catchments in Panama, this non-conservative behavior has been attributed to large intensity precipitation events as a result of pre-event water contributions becoming more dilute across the course of rainstorms (Litt et al., 2015). Another reason for discrepancies among flow components estimated using stable isotopes and EC could arise from spatial variability in the activation of different water flow paths contributing to discharge (Hoeg et al., 2000). Our findings indicate that these sources of discrepancy are overcome at our study site as a result of the presence of riparian wetlands presenting high porosity and available water storage capacity for tracer mixing (Lazo et al., 2019) in combination with low contributions of water from

Fig. 3. Best model performance metrics (KGE and AIC) of flow partitioning using high resolution $\delta^{18}O$ and EC data with each model structure. Red, blue, orange, and green bars correspond to model structures 1, 2, 3, and 4, respectively. Subplots a) and b) correspond to $\delta^{18}O$ calibration, and (c) and (d) correspond to EC calibration. (For interpretation of the references to colour in this figure legend, the reader is referred to the web version of this article.)

deeper groundwater flow paths (Correa et al., 2019, 2017; Mosquera et al., 2016a). These conditions likely reduce the spatial variability of EC across the catchment before reaching the stream (Mosquera et al., 2016b). These findings are further supported by the remarkably similar process-based understanding yielded by the model simulations regardless of the tracer used for calibration and flow conditions (from low to high), as evidenced by the strong similarity between the system's TTDs (Fig. 6). Altogether, these findings point to a quasi-conservative behavior of EC at the study area, making it suitable for monitoring rainfall-runoff processes at high-temporal frequency.

4.3. Increase in model performance using high resolution EC data

The lack of samples collected during peak flow in combination with a low sampling resolution (ratio of samples collected during an event to its duration in hours) caused discrepancies for the four events which presented PEWF differences>20% between $\delta^{18}O$ and EC (Fig. 5), particularly for long-duration events (>90 h). Our findings indicate that sampling resolution and the number of samples collected during high flows should increase to avoid missing critical information during peak flow production (von Freyberg et al., 2017), highlighting the importance of and need for high-resolution monitoring during rainfall-runoff events.

One of the main advantages of finding a tracer that can be monitored at high temporal frequency while satisfying the assumptions of the two-component hydrograph separation, is that it provides the opportunity to identify the variability of fast occurring rainfall-runoff processes. EC is an ideal alternative tracer considering its ease of in-stream measurement at fine temporal resolution (sub-hourly) and lower operational monitoring cost, compared to $\delta^{18}O$ (Cano-Paoli et al., 2019). In this context, our results clearly showed that when 5-minute EC data were used for model calibration the goodness of fit of the hydrograph and tracer data increased significantly for all monitored events. That is, KGE values increased an average of 0.16 in relation those obtained when using data collected at 1 to 6 h intervals (Fig. 7). These findings highlight the value of monitoring tracer data at high temporal frequency (Floury et al., 2017; Pesántez et al., 2021; Von Freyberg et al., 2017), so that the

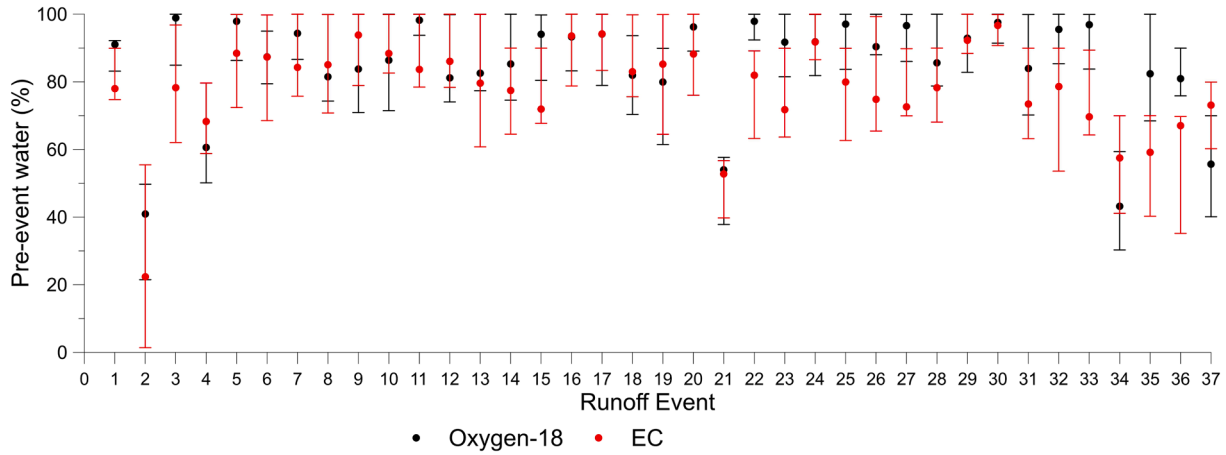

Fig. 4. Pre-event water fractions (PEWs) estimated using model structure 4 and calibrated for Oxygen-18 (black dots) and electrical conductivity (EC; red dots). Vertical lines represent uncertainty in PEWs corresponding to the 5–95% confidence limits of the possible solutions from the parameter sets within the range of behavioral solutions. (For interpretation of the references to colour in this figure legend, the reader is referred to the web version of this article.)

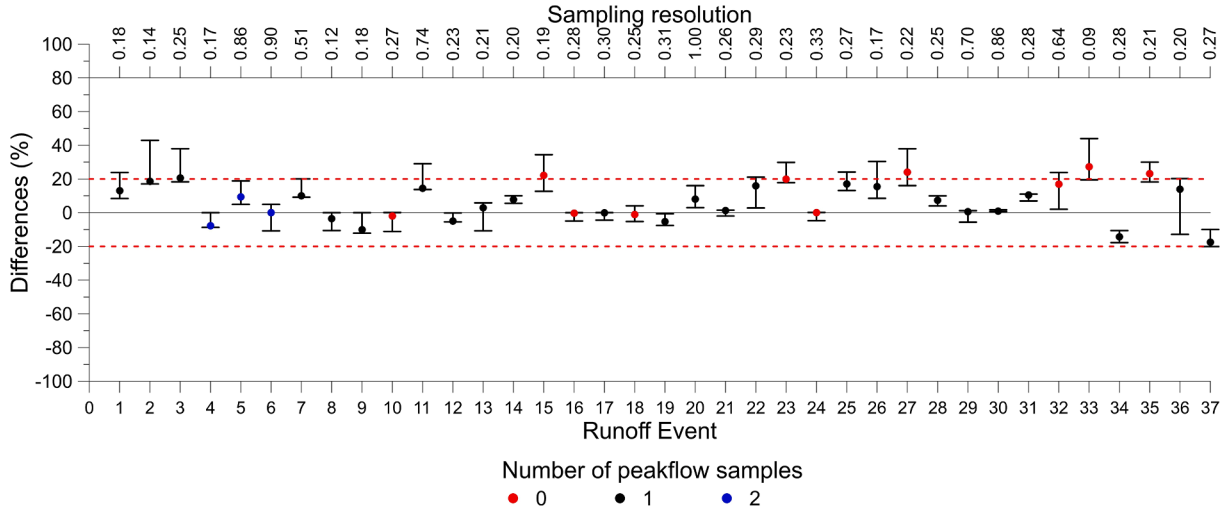

Fig. 5. Differences in pre-event water fractions (PEWs) estimated using Oxygen-18 and electrical conductivity for calibration of model structure 4. Dots represent the difference between the PEWs which produced the highest KGE vales for each tracer. Solid horizontal black line represents no difference (i.e., 0%). Dashed horizontal red lines represent the threshold for acceptable differences (±20%). Black vertical lines represent the differences in PEWs considering the estimated uncertainties determined for model calibration with each tracer (i.e., 5–95% confidence limits of behavioral solutions). The dots' colors correspond to events with 0 (red), 1 (black), and 2 (blue) water samples collected during peak flow. Sampling factor is equal to the total number of samples taken during an event divided by the duration of the event. (For interpretation of the references to colour in this figure legend, the reader is referred to the web version of this article.)

Table 2
Non-parametric tests for statistical differences between Oxygen-18 and EC modelling results for each model structure. Bold values represent p-values>0.05.

Model Structure	Sign Test p-value	Wilcoxon signed-rank test p-value	Power of the statistical test
1	**0.26**	**0.05**	0.83
2	**0.62**	**0.16**	0.75
3	**0.07**	**0.10**	0.95
4	**0.19**	**0.07**	0.96

temporal variability of water transport and mixing processes can be better identified (Mosquera et al., 2018; Stockinger et al., 2016; Timbe et al., 2015). Addressing this issue is especially important in environments with fast hydrological response, where peak flows often occur in time periods less than an hour (e.g., Sahraei et al., 2020); so that the lack of high-frequency data can result in a significant loss of information (Kirchner et al., 2004). According to our findings, high-frequency EC data can help overcome this issue in catchments with similar characteristics to ours, while providing robust flow partitioning results as evidenced by the comparative analysis between EC and stable isotopes presented above.

5. Conclusions

Our study showed that EC yielded similar results than $\delta^{18}O$ at event and pre-event hydrograph separation with a tracer-aided hydrological model covering a wide range of flow conditions (low to high peak flows), not only in amount of water but also at catchment internal processes representation as shown by the similarity of the TTDs when calibrating the model structures. These similarities could be attributed to some specific catchment characteristics such as high water storage capacity due to the high water retention capacity of the porous soils which allows for an efficient mixing of the water in the system, combined with low groundwater contributions that reduce the spatial variability of EC, resulting in a quasi-conservative behavior from this tracer. This behavior opens the possibility to use EC as an alternative tracer instead

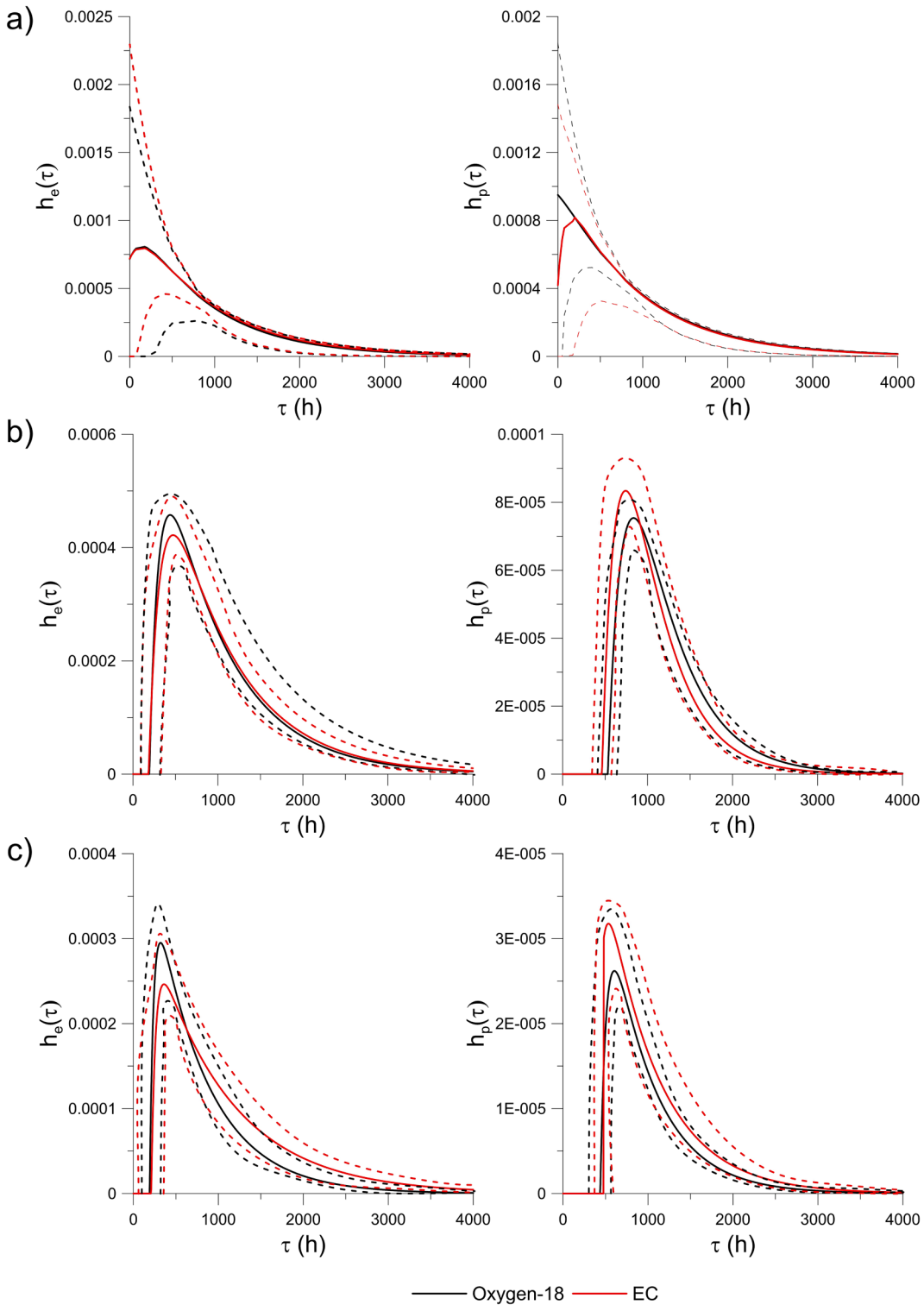

Fig. 6. Transit time distributions (TTDs) of event (he) and pre-event (hp) flow components for model structure 4 using Oxygen-18 and electrical conductivity (EC) for calibration for runoff event a) 4, b) 17, and c) 36. Solid lines represent TTDs based on the 50th percentiles of behavioral parameters sets. Dashed lines correspond to the 25th and 75th percentiles of behavioral parameters sets.

of stable isotopes ($\delta^{18}O$) in hydrograph separation studies, increasing the sampling resolution which will make it possible to have a quasi-continuous measurement of tracer data. This will help to increase the number of samples available for hydrograph separation analyses increasing the performance of models, resulting in an accurate representation of catchment hydrological behavior even at peak flow where information is often missing. This, in turn, could help to reveal fast occurring rainfall-runoff processes. In addition, EC could lower the resources needed to maintain high-frequency monitoring networks as it is easier to measure allowing a sustained acquisition of data in the long-term, which is often unachievable with other tracers (i.e., stable isotopes), especially in remote places were logistics are very difficult and financial support is scarce.

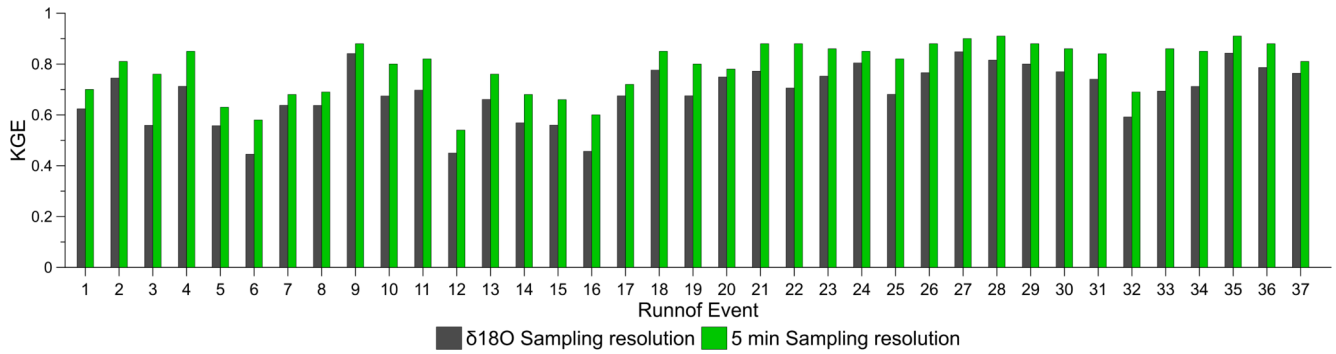

Fig. 7. Comparison of EC sampling resolution on the goodness of fit (in terms of the Kling Gupta Efficiency, KGE) of flow partitioning modelling using model structure 4 and data collected at 5-minute intervals and at the frequency δ18O data was available (1–6 h intervals) for the 37 rainfall-runoff events.

CRediT authorship contribution statement

Patricio X. Lazo: Conceptualization, Methodology, Formal analysis, Investigation, Writing – original draft, Writing – review & editing, Visualization. **Giovanny M. Mosquera:** Conceptualization, Resources, Writing – review & editing, Supervision, Funding acquisition. **Irene Cárdenas:** Investigation, Resources. **Catalina Segura:** Methodology, Software, Resources, Writing – review & editing, Supervision. **Patricio Crespo:** Conceptualization, Resources, Writing – review & editing, Supervision, Project administration, Funding acquisition.

Declaration of Competing Interest

The authors declare that they have no known competing financial interests or personal relationships that could have appeared to influence the work reported in this paper.

Data availability

Data will be made available on request.

Acknowledgements

This manuscript is an outcome of the University of Cuenca's Doctoral Program in Water Resources. The authors would like to thank INV Metals S.A. staff for their assistance in the logistics at the Zhurucay Ecohydrological Observatory. We also thank Franklin Marín, Juan Pesántez, Mishelle Palacios, Viviana Arízaga, Pablo Peña, Juan Cabrera, and Karina Larco for their support with the collection of water samples and hydrometeorological data.

Funding

This research was funded by the International Atomic Energy Agency (IAEA) and the Vice-rectorate of Investigation of the University of Cuenca (VIUC) through research contracts 22906 "Evaluation of Non-Stationary Hydrological Conditions in the Andean Páramo" and 22905 "Identification of Tap Water Sources and Water Supply Structure in a Mesoscale Tropical Andean City". G.M.M. is supported by a Postdoctoral Fellowship from the Universidad San Francisco de Quito and the H2020 European Research and Innovation action Grant Agreement N°869226 (DRYvER). C.S. was supported in part by the NSF Award No. 1943574.

Appendix A. Supplementary data

Supplementary data to this article can be found online at https://doi.org/10.1016/j.jhydrol.2022.128898.

References

Akaike, H., 1974. A new look at the statistical model identification. IEEE Trans. Automat. Contr. 19, 716–723. https://doi.org/10.1109/TAC.1974.1100705.

Benettin, P., Bailey, S.W., Campbell, J.L., Green, M.B., Rinaldo, A., Likens, G.E., McGuire, K.J., Botter, G., 2015. Linking water age and solute dynamics in streamflow at the Hubbard Brook Experimental Forest, NH, USA. Water Resour. Res. 51(11) 9256-9272. 51, 9256–9272. doi:10.1002/2015WR017552.

Benettin, P., Van Der Velde, Y., Van Der Zee, S.E.A.T.M., Rinaldo, A., Botter, G., 2013. Chloride circulation in a lowland catchment and the formulation of transport by travel time distributions. Water Resour. Res. 49, 4619–4632. https://doi.org/10.1002/WRCR.20309.

Beven, K., Freer, J., 2001. Equifinality, data assimilation, and uncertainty estimation in mechanistic modelling of complex environmental systems using the GLUE methodology. J. Hydrol. 249, 11–29. https://doi.org/10.1016/S0022-1694(01)00421-8.

Birkel, C., Tetzlaff, D., Dunn, S.M., Soulsby, C., 2011. Using lumped conceptual rainfall–runoff models to simulate daily isotope variability with fractionation in a nested mesoscale catchment. Adv. Water Resour. 34, 383–394. https://doi.org/10.1016/J.ADVWATRES.2010.12.006.

Birkel, C., Soulsby, C., Tetzlaff, D., 2014. Developing a consistent process-based conceptualization of catchment functioning using measurements of internal state variables. Water Resour. Res. 50, 3481–3501. https://doi.org/10.1002/2013WR014925.

Blume, T., Zehe, E., Bronstert, A., 2008. Investigation of runoff generation in a pristine, poorly gauged catchment in the Chilean Andes II: Qualitative and quantitative use of tracers at three spatial scales. Hydrol. Process. 22, 3676–3688. https://doi.org/10.1002/hyp.6970.

Bonell, M., Pearce, A.J., Stewart, M.K., 1990. The identification of runoff-production mechanisms using environmental isotopes in a tussock grassland catchment, eastern otago, New Zealand. Hydrol. Process. 4, 15–34. https://doi.org/10.1002/HYP.3360040103.

Buttle, J.M., 1994. Isotope hydrograph separations and rapid delivery of pre-event water from drainage basins. Prog. Phys. Geogr. Earth Environ. 18, 16–41. https://doi.org/10.1177/030913339401800102.

Camacho Suarez, V.V., Saraiva Okello, A.M.L., Wenninger, J.W., Uhlenbrook, S., Suarez, C., 2015. Understanding runoff processes in a semi-arid environment through isotope and hydrochemical hydrograph separations. Hydrol. Earth Syst. Sci 19, 4183–4199. https://doi.org/10.5194/hess-19-4183-2015.

Cano-Paoli, K., Chiogna, G., Bellin, A., 2019. Convenient use of electrical conductivity measurements to investigate hydrological processes in Alpine headwaters. Sci. Total Environ. 685, 37–49. https://doi.org/10.1016/J.SCITOTENV.2019.05.166.

Chapman, T., 1999. A comparison of algorithms for stream flow recession and baseflow separation. Hydrol. Process. 13, 701–714. https://doi.org/10.1002/(SICI)1099-1085(19990415)13:5<701::AID-HYP774>3.0.CO;2-2.

Christophersen, N., Hooper, R.P., 1992. Multivariate analysis of stream water chemical data: The use of principal components analysis for the end-member mixing problem. Water Resour. Res. 28, 99–107. https://doi.org/10.1029/91WR02518.

Córdova, M., Carrillo-Rojas, G., Crespo, P., Wilcox, B., Célleri, R., 2015. Evaluation of the Penman-Monteith (FAO 56 PM) Method for Calculating Reference Evapotranspiration Using Limited Data. Mt. Res. Dev. 35, 230–239. https://doi.org/10.1659/MRD-JOURNAL-D-14-0024.1.

Correa, A., Windhorst, D., Tetzlaff, D., Crespo, P., Célleri, R., Feyen, J., Breuer, L., 2017. Temporal dynamics in dominant runoff sources and flow paths in the Andean Páramo. Water Resour. Res. 53, 5998–6017. https://doi.org/10.1002/2016WR020187.

Correa, A., Breuer, L., Crespo, P., Célleri, R., Feyen, J., Birkel, C., Silva, C., Windhorst, D., 2019. Spatially distributed hydro-chemical data with temporally high-resolution is needed to adequately assess the hydrological functioning of headwater catchments. Sci. Total Environ. 651, 1613–1626. https://doi.org/10.1016/J.SCITOTENV.2018.09.189.

Crespo, P.J., Feyen, J., Buytaert, W., Bücker, A., Breuer, L., Frede, H.-G., Ramírez, M., 2011. Identifying controls of the rainfall–runoff response of small catchments in the

tropical Andes (Ecuador). J. Hydrol. 407, 164–174. https://doi.org/10.1016/j.jhydrol.2011.07.021.
Delsman, J.R., Essink, G.H.P.O., Beven, K.J., Stuyfzand, P.J., 2013. Uncertainty estimation of end-member mixing using generalized likelihood uncertainty estimation (GLUE), applied in a lowland catchment. Water Resour. Res. 49, 4792–4806. https://doi.org/10.1002/WRCR.20341.
Dunkerley, D., 2008. Identifying individual rain events from pluviograph records: a review with analysis of data from an Australian dryland site. Hydrol. Process. 22, 5024–5036. https://doi.org/10.1002/hyp.7122.
Esquivel-Hernández, G., Mosquera, G.M., Sánchez-Murillo, R., Quesada-Román, A., Birkel, C., Crespo, P., Célleri, R., Windhorst, D., Breuer, L., Boll, J., 2019. Moisture transport and seasonal variations in the stable isotopic composition of rainfall in Central American and Andean Páramo during El Niño conditions (2015–2016). Hydrol. Process. 33, 1802–1817. https://doi.org/10.1002/hyp.13438.
Floury, P., Gaillardet, J., Gayer, E., Bouchez, J., Tallec, G., Ansart, P., Koch, F., Gorge, C., Blanchouin, A., Roubaty, J.L., 2017. The potamochemical symphony: New progress in the high-frequency acquisition of stream chemical data. Hydrol. Earth Syst. Sci. 21, 6153–6165. https://doi.org/10.5194/HESS-21-6153-2017.
Forster, M.R., 2000. Key concepts in model selection: Performance and generalizability. J. Math. Psychol. 44, 205–231. https://doi.org/10.1006/JMPS.1999.1284.
Goller, R., Wilcke, W., Leng, M.J., Tobschall, H.J., Wagner, K., Valarezo, C., Zech, W., 2005. Tracing water paths through small catchments under a tropical montane rain forest in south Ecuador by an oxygen isotope approach. J. Hydrol. 308, 67–80. https://doi.org/10.1016/j.jhydrol.2004.10.022.
Gonzales, A.L., Nonner, J., Heijkers, J., Uhlenbrook, S., 2009. Comparison of different base flow separation methods in a lowland catchment. Hydrol. Earth Syst. Sci. 13, 2055–2068. https://doi.org/10.5194/HESS-13-2055-2009.
Guallpa, M., Célleri, R., Crespo, P., 2022. Efecto del coeficiente teórico de descarga de vertederos sobre la medición de caudales en pequeños ríos Andinos. La Granja 36. https://doi.org/10.17163/LGR.N36.2022.06.
Gupta, H.V., Kling, H., Yilmaz, K.K., Martinez, G.F., 2009. Decomposition of the mean squared error and NSE performance criteria: Implications for improving hydrological modelling. J. Hydrol. 377, 80–91. https://doi.org/10.1016/j.jhydrol.2009.08.003.
Hayashi, M., Vogt, T., Mächler, L., Schirmer, M., 2012. Diurnal fluctuations of electrical conductivity in a pre-alpine river: Effects of photosynthesis and groundwater exchange. J. Hydrol. 450–451, 93–104. https://doi.org/10.1016/J.JHYDROL.2012.05.020.
Hoeg, S., Uhlenbrook, S., Leibundgut, C., 2000. Hydrograph separation in a mountainous catchment ? combining hydrochemical and isotopic tracers. Hydrol. Process. 14, 1199–1216. https://doi.org/10.1002/(SICI)1099-1085(200005)14:7<1199::AID-HYP35>3.0.CO;2-K.
Hrachowitz, M., Bohte, R., Mul, M.L., Bogaard, T.A., Savenije, H.H.G., Uhlenbrook, S., 2011. On the value of combined event runoff and tracer analysis to improve understanding of catchment functioning in a data-scarce semi-arid area. Hydrol. Earth Syst. Sci. 15, 2007–2024. https://doi.org/10.5194/hess-15-2007-2011.
IUSS Working Group WRB, 2015. World Reference Base for Soil Resources 2014, update 2015. International soil classification system for naming soils and creating legends for soil maps. World Soil Resources Reports No. 106. FAO Rome.
Jakeman, A.J., Hornberger, G.M., 1993. How much complexity is warranted in a rainfall-runoff model? Water Resour. Res. 29, 2637–2649. https://doi.org/10.1029/93WR00877.
Kirchner, J.W., Feng, X., Neal, C., Robson, A.J., 2004. The fine structure of water-quality dynamics: the (high-frequency) wave of the future. Hydrol. Process. 18, 1353–1359. https://doi.org/10.1002/HYP.5537.
Klaus, J., McDonnell, J.J., 2013. Hydrograph separation using stable isotopes: Review and evaluation. J. Hydrol. 505, 47–64. https://doi.org/10.1016/j.jhydrol.2013.09.006.
Lang, M., Ouarda, T.B.M.J., Bobée, B., 1999. Towards operational guidelines for over-threshold modeling. J. Hydrol. https://doi.org/10.1016/S0022-1694(99)00167-5.
Laudon, H., Slaymaker, O., 1997. Hydrograph separation using stable isotopes, silica and electrical conductivity: an alpine example. J. Hydrol. 201, 82–101. https://doi.org/10.1016/S0022-1694(97)00030-9.
Laudon, H., Seibert, J., Köhler, S., Bishop, K., 2004. Hydrological flow paths during snowmelt: Congruence between hydrometric measurements and oxygen 18 in meltwater, soil water, and runoff. Water Resour. Res. 40 https://doi.org/10.1029/2003WR002455.
Lazo, P.X., Mosquera, G.M., McDonnell, J.J., Crespo, P., 2019. The role of vegetation, soils, and precipitation on water storage and hydrological services in Andean Páramo catchments. J. Hydrol. 572, 805–819. https://doi.org/10.1016/J.JHYDROL.2019.03.050.
Linsley, R.K., Kohler, M.A., Paulhus, J.L.H., 1982. Hydrology for engineers. Third edition.
Litt, G.F., Gardner, C.B., Ogden, F.L., Lyons, W.B., 2015. Hydrologic tracers and thresholds: A comparison of geochemical techniques for event-based stream hydrograph separation and flowpath interpretation across multiple land covers in the Panama Canal Watershed. Appl. Geochemistry 63, 507–518. https://doi.org/10.1016/J.APGEOCHEM.2015.04.003.
Lott, D.A., Stewart, M.T., 2016. Base flow separation: A comparison of analytical and mass balance methods. J. Hydrol. 535, 525–533. https://doi.org/10.1016/J.JHYDROL.2016.01.063.
Maloszewski, P., Zuber, A., 1996. Lumped parameter models for the interpretation of environmental tracer data, in Manual on Mathematical Models in Isotope Hydrogeology.
McDonnell, J.J., Bonell, M., Stewart, M.K., Pearce, A.J., 1990. Deuterium variations in storm rainfall: Implications for stream hydrograph separation. Water Resour. Res. 26, 455–458. https://doi.org/10.1029/WR026I003P00455.
McGlynn, B.L., McDonnell, J.J., 2003. Quantifying the relative contributions of riparian and hillslope zones to catchment runoff. Water Resour. Res. 39, n/a-n/a. https://doi.org/10.1029/2003WR002091.
McGuire, K.J., McDonnell, J.J., 2010. Hydrological connectivity of hillslopes and streams: Characteristic time scales and nonlinearities. Water Resour. Res. 46, 10543. https://doi.org/10.1029/2010WR009341.
McGuire, K.J., Weiler, M., McDonnell, J.J., 2007. Integrating tracer experiments with modeling to assess runoff processes and water transit times. Adv. Water Resour. 30, 824–837. https://doi.org/10.1016/j.advwatres.2006.07.004.
Mei, Y., Anagnostou, E.N., 2015. A hydrograph separation method based on information from rainfall and runoff records. J. Hydrol. 523, 636–649. https://doi.org/10.1016/J.JHYDROL.2015.01.083.
Meriano, M., Howard, K.W.F., Eyles, N., 2011. The role of midsummer urban aquifer recharge in stormflow generation using isotopic and chemical hydrograph separation techniques. J. Hydrol. 396, 82–93. https://doi.org/10.1016/J.JHYDROL.2010.10.041.
Michel, C., Perrin, C., Andreassian, V., 2003. The exponential store: a correct formulation for rainfall—runoff modelling. Hydrol. Sci. J. 48, 109–124. https://doi.org/10.1623/hysj.48.1.109.43484.
Miller, M.P., Susong, D.D., Shope, C.L., Heilweil, V.M., Stolp, B.J., 2014. Continuous estimation of baseflow in snowmelt-dominated streams and rivers in the Upper Colorado River Basin: A chemical hydrograph separation approach. Water Resour. Res. 50, 6986–6999. https://doi.org/10.1002/2013WR014939.
Moore, R.B., 2004. Introduction to salt dilution gauging for streamflow measurement Part 2: Constant-rate injection. Streamline Watershed Manag. Bluletin 8, 11–15.
Mosquera, G.M., Lazo, P.X., Célleri, R., Wilcox, B.P., Crespo, P., 2015. Runoff from tropical alpine grasslands increases with areal extent of wetlands. CATENA 125, 120–128. https://doi.org/10.1016/j.catena.2014.10.010.
Mosquera, G.M., Célleri, R., Lazo, P.X., Vaché, K.B., Perakis, S.S., Crespo, P., 2016a. Combined use of isotopic and hydrometric data to conceptualize ecohydrological processes in a high-elevation tropical ecosystem. Hydrol. Process. 30, 2930–2947. https://doi.org/10.1002/hyp.10927.
Mosquera, G.M., Segura, C., Vaché, K.B., Windhorst, D., Breuer, L., Crespo, P., 2016b. Insights into the water mean transit time in a high-elevation tropical ecosystem. Hydrol. Earth Syst. Sci. 20, 2987–3004. https://doi.org/10.5194/hess-20-2987-2016.
Mosquera, G., Segura, C., Crespo, P., Mosquera, G.M., Segura, C., Crespo, P., 2018. Flow Partitioning Modelling Using High-Resolution Isotopic and Electrical Conductivity Data. Water 10, 904. https://doi.org/10.3390/w10070904.
Muñoz-Villers, L.E., McDonnell, J.J., 2012. Runoff generation in a steep, tropical montane cloud forest catchment on permeable volcanic substrate. Water Resour. Res. 48, n/a-n/a. https://doi.org/10.1029/2011WR011316.
Munyaneza, O., Wenninger, J., Uhlenbrook, S., 2012. Identification of runoff generation processes using hydrometric and tracer methods in a meso-scale catchment in Rwanda. Hydrol. Earth Syst. Sci. 16, 1991–2004. https://doi.org/10.5194/HESS-16-1991-2012.
Ochoa-Sánchez, A., Crespo, P., Célleri, R., 2018. Quantification of rainfall interception in the high Andean tussock grasslands. Ecohydrology e1946. https://doi.org/10.1002/eco.1946.
Padrón, R.S., Wilcox, B.P., Crespo, P., Célleri, R., 2015. Rainfall in the Andean Páramo: New Insights from High-Resolution Monitoring in Southern Ecuador. J. Hydrometeorol. 16, 985–996. https://doi.org/10.1175/JHM-D-14-0135.1.
Pearce, A.J., Stewart, M.K., Sklash, M.G., 1986. Storm Runoff Generation in Humid Headwater Catchments: 1. Where Does the Water Come From? Water Resour. Res. 22, 1263–1272. https://doi.org/10.1029/WR022i008p01263.
Pellerin, B.A., Wollheim, W.M., Feng, X., Vörösmarty, C.J., 2008. The application of electrical conductivity as a tracer for hydrograph separation in urban catchments. Hydrol. Process. 22, 1810–1818. https://doi.org/10.1002/hyp.6786.
Penna, D., Stenni, B., Šanda, M., Wrede, S., Bogaard, T.A., Michelini, M., Fischer, B.M.C., Gobbi, A., Mantese, N., Zuecco, G., Borga, M., Bonazza, M., Sobotková, M., Čejková, B., Wassenaar, L.I., 2012. Technical note: Evaluation of between-sample memory effects in the analysis of δ2H and δ18O of water samples measured by laser spectroscopes. Hydrol. Earth Syst. Sci. 16, 3925–3933. https://doi.org/10.5194/hess-16-3925-2012.
Penna, D., van Meerveld, H.J., Oliviero, O., Zuecco, G., Assendelft, R.S., Fontana, G.D., Borga, M., 2015. Seasonal changes in runoff generation in a small forested mountain catchment. Hydrol. Process. 29, 2027–2042. https://doi.org/10.1002/HYP.10347.
Pesántez, J., Birkel, C., Mosquera, G.M., Peña, P., Arízaga-Idrovo, V., Mora, E., McDowell, W.H., Crespo, P., 2021. High-frequency multi-solute calibration using an in situ UV–visible sensor. Hydrol. Process. 35, e14357.
Pfister, L., Kirchner, J.W., 2017. Debates—Hypothesis testing in hydrology: Theory and practice. Water Resour. Res. 53, 1792–1798. https://doi.org/10.1002/2016WR020116.
Quichimbo, P., Tenorio, G., Borja, P., Cárdenas, I., Crespo, P., Célleri, R., 2012. Efectos sobre las propiedades físicas y químicas de los suelos por el cambio de la cobertura vegetal y uso del suelo: Páramo de Quimsacocha al sur del Ecuador. Suelos Ecuatoriales 42, 138–153.
Ribatet, M., Dutang, C., 2004. Generalized Pareto Distribution and Peaks Over Threshold.
Romanowicz, R., 2010. An application of a log-transformed low-flow (LTLF) model to baseflow separation. https://doi.org/10.1080/02626667.2010.505172 55, 952–964. doi:10.1080/02626667.2010.505172.
Sahraei, A., Kraft, P., Windhorst, D., Breuer, L., 2020. High-Resolution, In Situ Monitoring of Stable Isotopes of Water Revealed Insight into Hydrological Response Behavior. Water 12, 565. https://doi.org/10.3390/w12020565.

Saraiva Okello, A.M.L., Uhlenbrook, S., Jewitt, G.P.W., Masih, I., Riddell, E.S., Van der Zaag, P., 2018. Hydrograph separation using tracers and digital filters to quantify runoff components in a semi-arid mesoscale catchment. Hydrol. Process. 32, 1334–1350. https://doi.org/10.1002/HYP.11491.

Segura, C., James, A.L., Lazzati, D., Roulet, N.T., 2012. Scaling relationships for event water contributions and transit times in small-forested catchments in Eastern Quebec. Water Resour. Res. 48, n/a-n/a. https://doi.org/10.1029/2012WR011890.

Shope, C.L., 2016. Disentangling event-scale hydrologic flow partitioning in mountains of the Korean Peninsula under extreme precipitation. J. Hydrol. 538, 399–415. https://doi.org/10.1016/j.jhydrol.2016.04.050.

Sklash, M.G., Farvolden, R.N., 1979. The role of groundwater in storm runoff. J. Hydrol. 43, 45–65. https://doi.org/10.1016/0022-1694(79)90164-1.

Soulsby, C., Birkel, C., Geris, J., Dick, J., Tunaley, C., Tetzlaff, D., 2015. Stream water age distributions controlled by storage dynamics and nonlinear hydrologic connectivity: Modeling with high-resolution isotope data. Water Resour. Res. 51, 7759–7776. https://doi.org/10.1002/2015WR017888.

Sprent, P., 2011. Sign Test, in: International Encyclopedia of Statistical Science. Springer Berlin Heidelberg, Berlin, Heidelberg, pp. 1316–1317. doi:10.1007/978-3-642-04898-2_515.

St Amour, N.A., Gibson, J.J., Edwards, T.W.D., Prowse, T.D., Pietroniro, A., 2005. Isotopic time-series partitioning of streamflow components in wetland-dominated catchments, lower Liard River basin, Northwest Territories. Canada. Hydrol. Process. 19, 3357–3381. https://doi.org/10.1002/HYP.5975.

Stadnyk, T.A., Delavau, C., Kouwen, N., Edwards, T.W.D., 2013. Towards hydrological model calibration and validation: simulation of stable water isotopes using the isoWATFLOOD model. Hydrol. Process. 27, 3791–3810. https://doi.org/10.1002/HYP.9695.

Stewart, M., Cimino, J., Ross, M., 2007. Calibration of Base Flow Separation Methods with Streamflow Conductivity. Groundwater 45, 17–27. https://doi.org/10.1111/J.1745-6584.2006.00263.X.

Stockinger, M.P., Bogena, H.R., Lücke, A., Diekkrüger, B., Cornelissen, T., Vereecken, H., 2016. Tracer sampling frequency influences estimates of young water fraction and streamwater transit time distribution. J. Hydrol. 541, 952–964. https://doi.org/10.1016/J.JHYDROL.2016.08.007.

Su, C.H., Costelloe, J.F., Peterson, T.J., Western, A.W., 2016. On the structural limitations of recursive digital filters for base flow estimation. Water Resour. Res. 52, 4745–4764. https://doi.org/10.1002/2015WR018067.

Timbe, E., Windhorst, D., Celleri, R., Timbe, L., Crespo, P., Frede, H.G., Feyen, J., Breuer, L., 2015. Sampling frequency trade-offs in the assessment of mean transit times of tropical montane catchment waters under semi-steady-state conditions. Hydrol. Earth Syst. Sci. 19, 1153–1168. https://doi.org/10.5194/HESS-19-1153-2015.

Tomczak, M., Tomczak, E., 2014. The need to report effect size estimates revisited. An overview of some recommended measures of effect size, Trends Sport Sci, p. 1.

Tweed, S., Munksgaard, N., Marc, V., Rockett, N., Bass, A., Forsythe, A.J., Bird, M.I., Leblanc, M., 2016. Continuous monitoring of stream δ18O and δ2H and stormflow hydrograph separation using laser spectrometry in an agricultural catchment. Hydrol. Process. 30, 648–660. https://doi.org/10.1002/HYP.10689.

U.S. Bureau of Reclamation, Water Measurement Manual 2001 Washington DC.

Vaché, K.B., McDonnell, J.J., 2006. A process-based rejectionist framework for evaluating catchment runoff model structure. Water Resour. Res. 42, 2409. https://doi.org/10.1029/2005WR004247.

Vidon, P., Cuadra, P.E., 2010. Impact of precipitation characteristics on soil hydrology in tile-drained landscapes. Hydrol. Process. 24, 1821–1833. https://doi.org/10.1002/HYP.7627.

Von Freyberg, J., Studer, B., Kirchner, J.W., 2017. A lab in the field: High-frequency analysis of water quality and stable isotopes in stream water and precipitation. Hydrol. Earth Syst. Sci. 21, 1721–1739. https://doi.org/10.5194/hess-21-1721-2017.

Wang, L., van Meerveld, H.J., Seibert, J., 2018. Effect of Observation Errors on the Timing of the Most Informative Isotope Samples for Event-Based Model Calibration. Hydrol. 2018, Vol. 5, Page 4 5, 4. doi:10.3390/HYDROLOGY5010004.

Wang, L., van Meerveld, H.J., Seibert, J., 2017. When should stream water be sampled to be most informative for event-based, multi-criteria model calibration? Hydrol. Res. 48, 1566–1584. https://doi.org/10.2166/nh.2017.197.

Wang, L., von Freyberg, J., van Meerveld, I., Seibert, J., Kirchner, J.W., 2019. What is the best time to take stream isotope samples for event-based model calibration? J. Hydrol. 577, 123950 https://doi.org/10.1016/J.JHYDROL.2019.123950.

Weiler, M., McGlynn, B.L., McGuire, K.J., McDonnell, J.J., 2003. How does rainfall become runoff? A combined tracer and runoff transfer function approach. Water Resour. Res. 39, n/a-n/a. https://doi.org/10.1029/2003WR002331.

Wilcoxon, F., 1945. Individual Comparisons by Ranking Methods. Biometrics Bull. 1, 80. https://doi.org/10.2307/3001968.

Wittenberg, H., 1999. Baseflow recession and recharge as nonlinear storage processes. Hydrol. Process. 13, 715–726. https://doi.org/10.1002/(SICI)1099-1085(19990415)13:5<715::AID-HYP775>3.0.CO;2-N.

Wittenberg, H., Sivapalan, M., 1999. Watershed groundwater balance estimation using streamflow recession analysis and baseflow separation. J. Hydrol. 219, 20–33. https://doi.org/10.1016/S0022-1694(99)00040-2.

Zhang, J., Zhang, Y., Song, J., Cheng, L., 2017. Evaluating relative merits of four baseflow separation methods in Eastern Australia. J. Hydrol. 549, 252–263. https://doi.org/10.1016/J.JHYDROL.2017.04.004.